Brodogradnja Volume 75, Number 3 (2024) 75305

journal homepage: www.brodogradnja.fsb.hr

Brodogradnja

An International Journal of Naval Architecture and Ocean Engineering for Research and Development

Study on numerical simulation and mitigation of parametric rolling in a container ship under head waves

Liu Liang[1], Zhang Baoji[1], Zhang Hao[2], Gong Jiaye[1], Tian Zheng[1], Guo Shuhui[1], Bao Yuanbiao[2], Zheng Xu[2]*

[1] *College of Ocean Science and Engineering, Shanghai Maritime University, Shanghai, 201306, China*
[2] *Merchant Marine College, Shanghai Maritime University, Shanghai, 201306, China*

ARTICLE INFO

Editor-in-Chief: Prof. Nastia Degiuli
Associate Editor: PhD Ivana Martić

Keywords:
Parametric rolling
CFD
Head wave
Container ship
Dynamic overset

ABSTRACT

To investigate the parametric rolling motion of container ships navigating in head seas, this study utilizes the unsteady RANS approach combined with dynamic overlapping grid technology to simulate parametric roll in a container ship under the coupled motions of roll, pitch, and heave. Initially, the model was validated against experimental results, demonstrating good agreement and thus confirming the reliability of the computational method. Furthermore, the paper investigates the impacts of the initial roll angle, encounter frequency, and the addition of bilge keels on parametric rolling. The research findings indicate that the initial angles of rolling impact the duration needed to attain a steady roll condition, yet they have minimal effect on the amplitude post-stabilization. The likelihood of parametric rolling arises when the frequency of encounters doubles that of the ship's inherent roll frequency. Furthermore, the likelihood of parametric rolling escalates when the wavelengths approach the length of the ship. Installing bilge keels markedly reduces the parametric rolling movement in vessels, and the occurrence of parametric rolling is also delayed.

1. Introduction

In recent years, the phenomenon of capsizing due to parametric rolling during a ship navigating in head seas has increasingly become a significant concern in the realm of maritime safety [1]. Parametric roll, as a complex dynamic response, has a particularly notable impact on ship stability, especially under severe sea conditions. With the rise in related maritime disasters, a thorough exploration and understanding of the physical mechanisms behind this phenomenon and accurate forecasting of such events are crucial for enhancing the safety and seaworthiness of ship designs, holding significant theoretical and practical implications.

Currently, there are three primary methods for forecasting parametric roll in ships: model testing, potential flow methods, and CFD methods based on viscous flow theory. Sergio et al. [2] employed a time-domain nonlinear six-degree-of-freedom numerical model of ship motion to forecast parametric roll under

* Corresponding author.
E-mail address: bjzhang@shmtu.edu.cn

http://dx.doi.org/10.21278/brod75305
Submitted 20 May 2024; Accepted 24 June 2024
ISSN 0007-215X; eISSN 1845-5859

regular wave conditions for a container ship, highlighting the influencing factors of parametric roll motion. Chen et al. [3] segmented the fluid domain into internal and external parts and developed a three-dimensional multi-domain higher-order boundary element method for solving the time-domain motion of ships in waves and the corresponding wave-induced resistance. Li et al. [4] proposed a numerical method based on potential flow theory and the boundary element method, which effectively addresses the motion and rolling of ships in waves. Silva et al. [5], based on time-domain potential flow theory, studied the impact of parametric rolling under both regular and irregular wave conditions on container ships navigating in head seas. Hu et al. [6] introduced a nonlinear numerical model considering the coupled three degrees of freedom of roll, pitch, and heave and conducted numerical forecasting of parametric roll motion for the C11 container ship in head-on regular waves. Coslovich [7] utilized a completely nonlinear potential flow method to analyze the parametric rolling motion of a container ship, incorporating a viscous damping coefficient in the roll motion equations to account for fluid viscosity effects. Ghamari [8] employed a hybrid time-domain wave solver combined with model experiments to study the conditions and motion characteristics of parametric rolling in a fishing vessel. The results indicate that ships exhibit a strong 6-DOF system behavior under parametric roll conditions, with roll coupled with other motion modes.

Potential flow theory posits that fluids are incompressible and viscosity is negligible, which restricts its accuracy in scenarios involving intense nonlinear effects, such as ships rolling on high seas. Zhou et al. [9] developed a hybrid approach combining three-dimensional potential flow theory and CFD methods to predict ship parametric roll motion, which was validated against experimental results. Their research indicates that the hybrid method can accurately predict roll damping. Burak et al. [10-12] estimated the impact of roll amplitude on roll damping using CFD methods and conducted comparative studies with ship model tests, demonstrating the efficacy of their approach. Wang et al. [13-15] employed CFD methods to analyze the roll motion of the KCS vessel model, investigating the conditions under which parametric rolling occurs and elucidating the mechanism behind it. Liu et al. [16] utilized the unsteady RANS method to perform numerical simulations of parametric roll on the surface combatant ONRT, discussing the influence of scale effects. Their findings suggest that scale effects on parametric roll are negligible. Subsequently, Liu et al. [17] also explored the impact of tank liquid sloshing on parametric roll, revealing that fluid motion could significantly reduce the natural roll frequency of the ship model, resulting in a narrower speed range for parametric rolling compared to models without sloshing.

Model testing is currently the most reliable method for studying ship parametric roll motion. Schumacher et al. [18-20] conducted experimental research on the parametric roll motion of container ships under regular and irregular wave conditions, identifying the conditions that lead to parametric rolling in container ships. Yu et al. [21] validated the effectiveness of a parametric roll early warning algorithm through model experiments and studied the impact of rudder-based roll reduction at high speeds. Kapsenberg et al. [22] performed direct stability assessments of parametric rolling on a container ship using model testing methods. They compared the ship model experimental results with numerical simulation outcomes using both probabilistic and deterministic approaches. Zhou et al. [23] focused on an Offshore Research Vessel, using model testing to explore the effects of nonlinear deck wetting on parametric roll and conducted comparative analyses with potential flow and CFD methods. Pesman et al. [24] investigated the effects of acceleration and deceleration in head seas with regular waves on parametric roll motion through model testing and developed a mathematical model to solve and validate their findings.

This paper employs CFD methods combined with dynamic overset grid technology to conduct numerical simulations of parametric rolling for a container ship navigating in the head sea. Initially, the reliability of the computational methods was validated through comparison with experimental data. Subsequently, the impact of initial roll angles and encounter frequencies on parametric rolling was discussed. Finally, the study examined the damping effects of bilge keels on parametric rolling.

2. Computational method

2.1 Governing equations

During numerical simulations of parametric rolling, the fluid surrounding the ship is considered to be an incompressible and viscous medium. Therefore, the unsteady RANS equations are solved in the water phase, and can be expressed in Cartesian coordinates as follows:

$$\frac{\partial(\rho u)}{\partial x}+\frac{\partial(\rho v)}{\partial y}+\frac{\partial(\rho w)}{\partial z}=0 \tag{1}$$

$$\begin{aligned}
&\frac{\partial(\rho u)}{\partial t}+\frac{\partial(\rho u^2)}{\partial x}+\frac{\partial(\rho uv)}{\partial y}+\frac{\partial(\rho uw)}{\partial z}=\rho f_x-\frac{\partial p}{\partial x}+\frac{\partial \tau_{xx}}{\partial x}+\frac{\partial \tau_{yx}}{\partial y}+\frac{\partial \tau_{zx}}{\partial z}\\
&\frac{\partial(\rho v)}{\partial t}+\frac{\partial(\rho uv)}{\partial x}+\frac{\partial(\rho v^2)}{\partial y}+\frac{\partial(\rho vw)}{\partial z}=\rho f_y-\frac{\partial p}{\partial y}+\frac{\partial \tau_{xy}}{\partial x}+\frac{\partial \tau_{yy}}{\partial y}+\frac{\partial \tau_{zy}}{\partial z}\\
&\frac{\partial(\rho w)}{\partial t}+\frac{\partial(\rho wu)}{\partial x}+\frac{\partial(\rho wv)}{\partial y}+\frac{\partial(\rho w^2)}{\partial z}=\rho f_z-\frac{\partial p}{\partial z}+\frac{\partial \tau_{xz}}{\partial x}+\frac{\partial \tau_{yz}}{\partial y}+\frac{\partial \tau_{zz}}{\partial z}
\end{aligned} \tag{2}$$

where u, v, w are the velocity components in the x, y, and z directions, respectively; ρ, p, f_i, and $\tau_{i,j}$ are the fluid density, the pressure, body force, and viscosity stress, respectively.

This study utilizes two sets of coordinate systems: the Earth-fixed coordinate system and the ship-fixed coordinate system, as illustrated in Fig. 1. The positive directions of X, Y, and Z respectively represent upstream, port side, and vertically upwards from the ship baseline. The motion of the ship is described within the Earth-fixed coordinate system. The ship-fixed coordinate system is attached to the ship's center of gravity, with its movements following those of the ship.

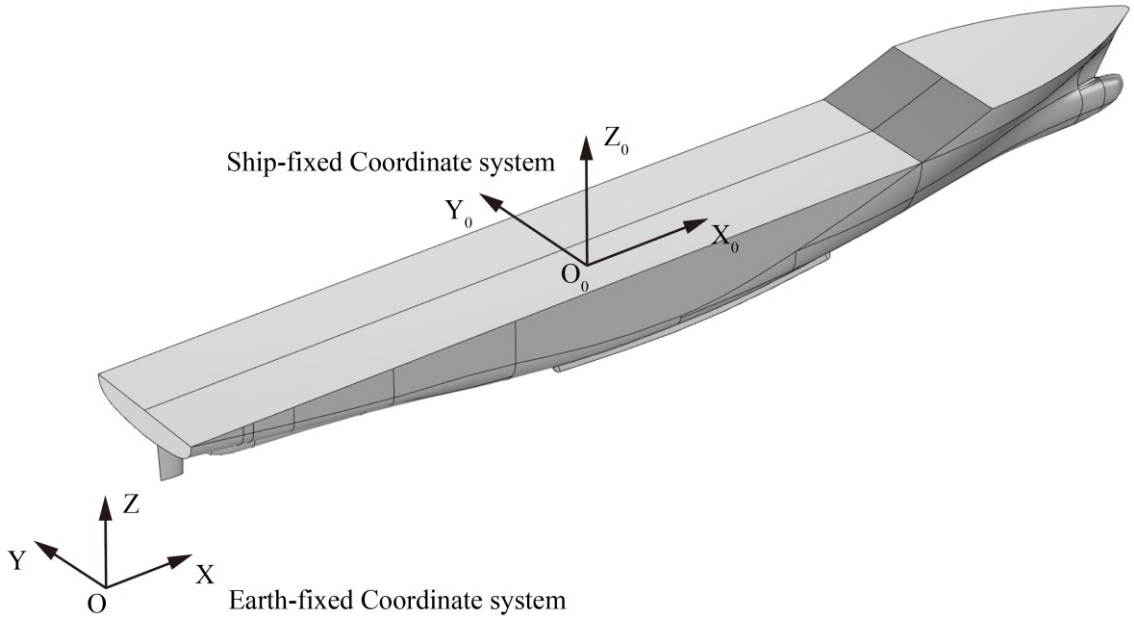

Fig. 1 Coordinate systems

2.2 Turbulence model

The closure of the governing equations is accomplished using the two-equation *SST* $k-\omega$ turbulence model presented by Menter. This turbulence model provides a reasonable solution for near-wall phenomena and effectively addresses issues associated with adverse pressure gradients and flow separation. Pena et al.

[25, 26], in their predictions of a ship's hydrodynamic performance, found that forecasts using the $SST\ k-\omega$ turbulence model exhibited smaller discrepancies with experimental measurements compared to those using the $k-\varepsilon$ turbulence model. Compared to the $k-\varepsilon$ model, the $SST\ k-\omega$ model better captures the wake field and boundary layer. Therefore, this paper employs the $SST\ k-\omega$ turbulence model to study the phenomenon of parametric rolling in ships. Turbulence variables are considered as a superposition of time-averaged and fluctuating components.

$$u_i = \overline{u}_i + u_i^{'} \tag{3}$$

$$p = \overline{p} + p' \tag{4}$$

Equations (3) and (4) are substituted into equations (1) and (2), allowing the control equations of the RANS model to be reformulated as follows:

$$\frac{\partial \overline{u}_i}{\partial x_i} = 0 \tag{5}$$

$$\frac{\partial}{\partial x_j}\left(\rho \overline{u}_i \overline{u}_j\right) = -\frac{\partial \overline{p}}{\partial x_i} + \frac{\partial}{\partial x_j}\left[\mu\left(\frac{\partial \overline{u}_i}{\partial x_j} + \frac{\partial \overline{u}_j}{\partial x_i}\right) - \rho\overline{u_i^{'} u_j^{'}}\right] \tag{6}$$

where $\rho\overline{u_i^{'} u_j^{'}}$ represents the Reynolds stress term.

The transport equations for turbulent kinetic energy and turbulence dissipation rate are as follows:

$$\frac{\partial k}{\partial t} + u_i \frac{\partial k}{\partial x_i} = \frac{\partial}{\partial x_j}\left[\left(\nu + \sigma_k \nu_t\right)\frac{\partial k}{\partial x_j}\right] + \tilde{P}_k - \beta^* k\omega + S_k \tag{7}$$

$$\frac{\partial \omega}{\partial t} + u_i \frac{\partial \omega}{\partial x_i} = \frac{\partial}{\partial x_j}\left[\left(\nu + \sigma_k \nu_t\right)\frac{\partial \omega}{\partial x_j}\right] + aS^2 - \beta\omega^2 + 2\left(1-F_1\right)\sigma_{\omega 2}\frac{1}{\omega}\frac{\partial k}{\partial x_j}\frac{\partial \omega}{\partial x_j} + S_\omega \tag{8}$$

where ν_t denotes the turbulent viscosity coefficient, while σ_k and σ_ω represents the turbulent Prandtl numbers for the transport equations of turbulent kinetic energy and turbulence dissipation rate, respectively. F_1 and F_2 are blending functions, with their calculation formulas presented as follows:

$$\nu_t = \frac{\alpha_1 k}{\max\left(\alpha_1 \omega, \Omega F_2\right)} \tag{9}$$

$$\sigma_k = \frac{1}{F_1 / \sigma_{k1} + \left(1-F_1\right)/\sigma_{k2}} \tag{10}$$

$$\sigma_\omega = \frac{1}{F_1 / \sigma_{\omega 1} + \left(1-F_1\right)/\sigma_{\omega 2}} \tag{11}$$

$$F_1 = \tan\left(\left(\min\left[\max\left(\frac{\sqrt{k}}{\beta^* \omega y}, \frac{500\nu}{y^2\omega}\right), \frac{4\rho\sigma_{\omega 2} k}{CD_{k\omega} y^2}\right]\right)^4\right) \tag{12}$$

$$F_2 = \tan\left(\left(\max\left(\frac{2\sqrt{k}}{\beta^* \omega y}, \frac{500\nu}{y^2\omega}\right)\right)^4\right) \tag{13}$$

where α_1, α_2, β_1, β_2, β^*, σ_{k1}, σ_{k2}, $\sigma_{\omega 1}$, and $\sigma_{\omega 2}$ represent model constants, with empirical values respectively assigned as 0.555, 0.44, 0.075, 0.828, 0.09, 0.85, 1, 0.5, and 0.856.

2.3 VOF method

Accurately tracking and describing the motion of the fluid-free surface during numerical simulations is crucial when employing Computational Fluid Dynamics methods to solve for ship motion. The Volume of Fluid (VOF) method, proposed by Hirt and Nichols, is a highly effective technique for free surface tracking [27]. The VOF method determines the free surface by calculating the volume fraction of one or more fluids within the grid cells. For the q phase, its equation can be expressed as follows:

$$\frac{\partial f_q}{\partial t} + \frac{\partial (u f_q)}{\partial x} + \frac{\partial (v f_q)}{\partial y} + \frac{\partial (w f_q)}{\partial z} = 0 \tag{14}$$

where $f_q = 1$ indicates that the grid cell is entirely occupied by water; $f_q = 0$ signifies that the grid cell is completely filled with air; when $0 < f_q < 1$ the grid cell represents the free surface.

3. Modeling and computational setup

3.1 KCS geometry

This study focuses on the KRISO Container Ship as depicted in Fig. 2 and Fig.3, employing CFD methods to forecast the ship's parametric roll movement. Yu et al. [28] conducted parametric roll experiments on the KCS vessel under regular wave conditions at the Towing Tank of Pusan National University. Their experimental data serve as validation for this research. The experimental model was scaled down to a ratio of 1:100, and the principal dimensions of the vessel are shown in Table 1.

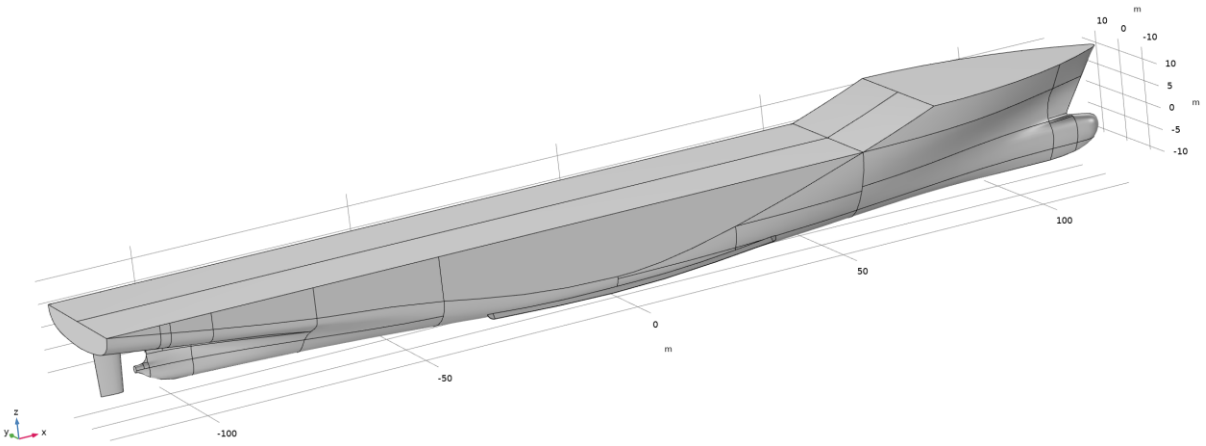

Fig. 2 Isometric side view and fundamental dimensions of the KCS ship

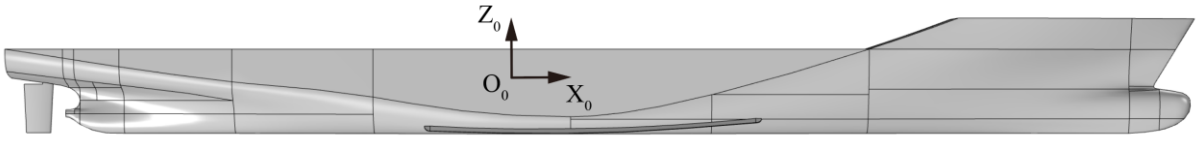

Fig. 3 Side view of the KCS model

Table 1 Geometrical particulars of KCS.

Project	Full scale	Model Scale
Length between perpendiculars, L_{PP} (m)	230	2.300
Breadth, B (m)	32.20	0.322
Depth, D_H (m)	19.0	0.190
Draft, d (m)	10.8	0.108
Displacement (m^3)	52030	0.052
Mass (kg)	—	52.030
Longitudinal position of Center of Buoyancy, LCB(m)	111.6	1.116
Metacentric height, GM(m)	1.290	0.0127
Radius of gyration, roll, K_{XX}/B	0.346	0.3242
Radius of gyration, pitch, yaw, K_{XX}/L_{PP}, K_{ZZ}/L_{PP}	0.248	0.2495

3.2 Computational region and grid

The accuracy of computation for parametric roll motion using the CFD method is greatly influenced by the calculation area, the settings of boundary conditions, and the division of the grid, all of which require judicious selection based on the research subject. In this study, a rectangular computational domain is utilized to resolve the flow field around the hull under parametric roll conditions, with the domain and boundary conditions depicted in Fig. 4. Within the ship-fixed coordinate system, the dimensions of the computational domain are $-3.5L_{PP} < X < 2.5L_{PP}$, $-2.0L_{PP} < Y < 2.0L_{PP}$, $-1.5L_{PP} < Z < 1.2L_{PP}$. Regarding the setup of boundary conditions, a zero-pressure gradient velocity inlet condition describes the far-field flow, while a pressure outlet condition is used at the exit. Wave damping is additionally implemented at all boundaries of the computational domain, except for the top and bottom, to mitigate the impact of wave reflection on the flow field surrounding the hull. Furthermore, a no-slip wall boundary condition is applied on the surfaces of the ship model and its appendages. The VOF method is employed to solve for the free surface during the simulation process.

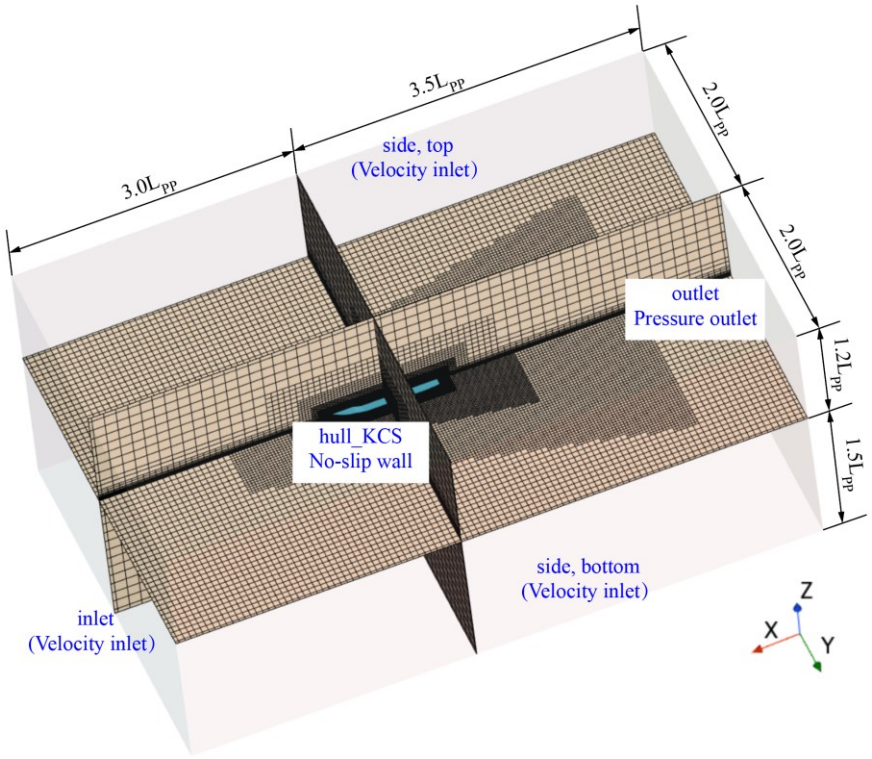

Fig. 4 Configuration of the calculation region and boundary conditions

The flow field calculation region is discretized using an unstructured hexahedral mesh. Details of the mesh around the hull are illustrated in Fig. 5. Regions close to the hull and the waterline employ a denser mesh to capture the free surface waveforms, with 50 mesh nodes per wavelength and 20 mesh nodes per wave height. Additionally, mesh refinement is also applied in areas near the bow, stern, rudder, and bilge keel to enhance the resolution of the flow field capture. Details of the mesh at the bow and stern are shown in Fig. 6.

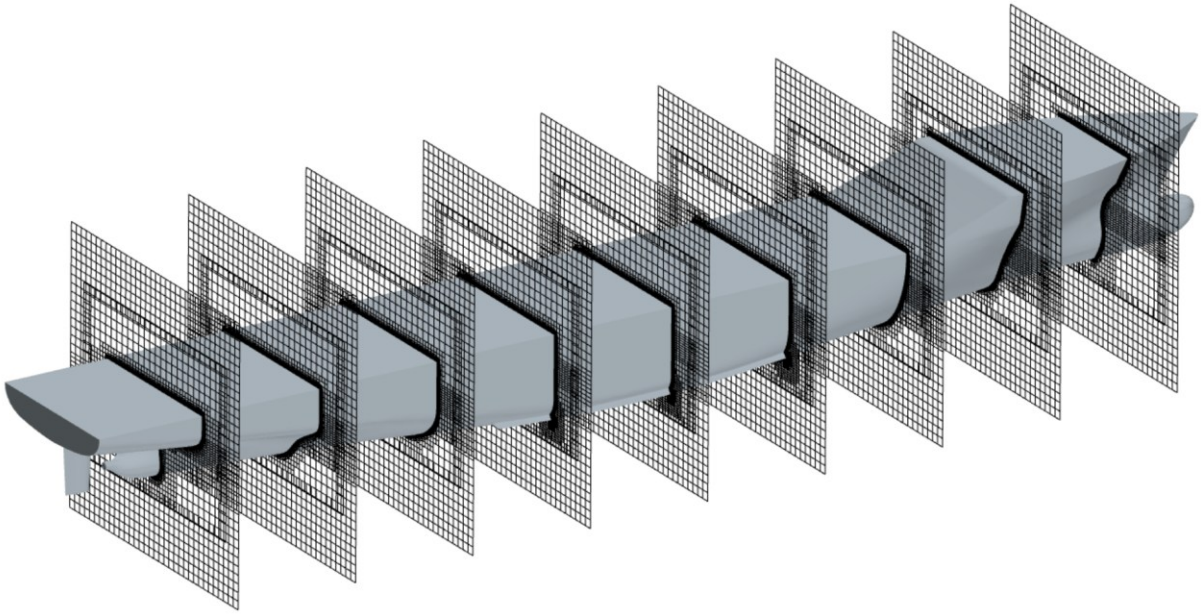

Fig. 5 Detailed grid configuration in the vicinity of the hull

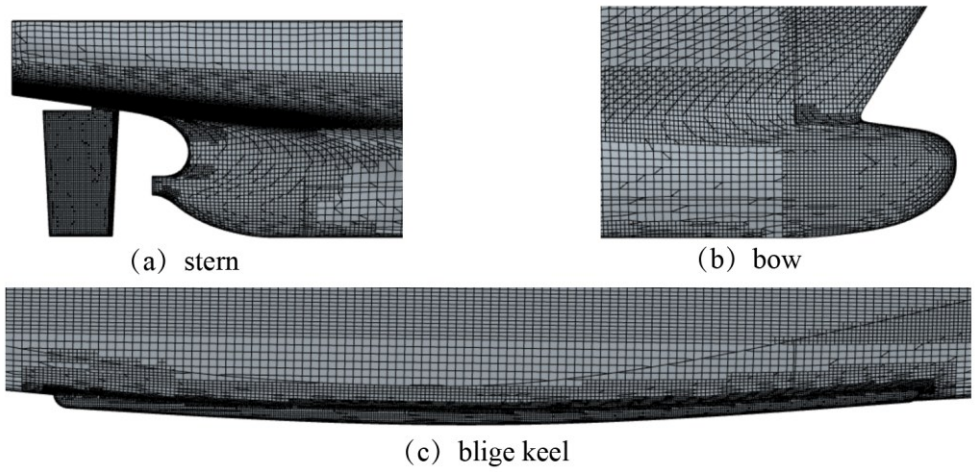

Fig. 6 Detailed grid configuration in the vicinity of the bow, stern, and bilge keels

Initially, it is necessary to validate the quality of the simulated wave elevations in the computational domain without the ship present ($\lambda/L_{PP} = 1$, $H_W/L_{PP} = 0.02$). To track the wave height over time, a stationary wave probe positioned 1.0 L_{PP} away from the inlet boundary is employed. Fig. 7 presents the CFD-calculated wave height time histories compared to theoretical estimates. The CFD outcomes closely align with the theoretical analyses.

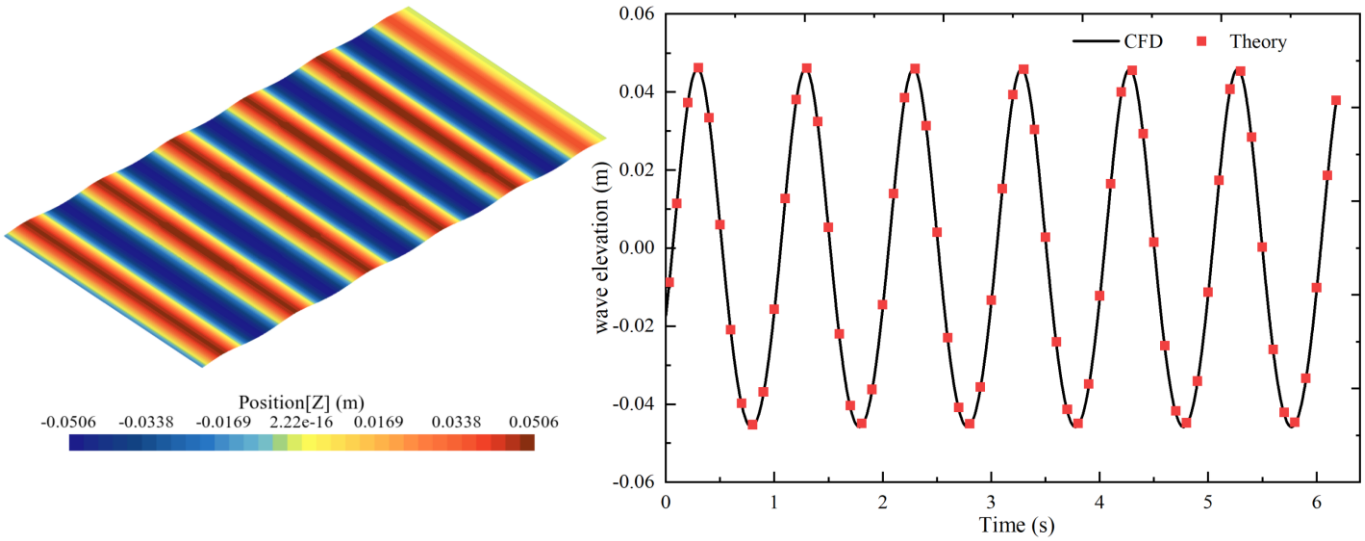

Fig. 7 Time histories of wave heights using CFD simulations against theoretical calculations

Within the boundary layer, the mesh spacing of the model is determined by the dimensionless wall span y^+, and can be expressed as follows:

$$y^+ = \frac{\rho u^k}{\mu} y \tag{15}$$

where the friction velocity is denoted by u^k, y represents the coordinate normal to the wall, and μ is the kinematic viscosity of the fluid. The $SST\ k-\omega$ turbulence model is employed to resolve the flow in the near-wall region of the hull. Consequently, the boundary layer mesh is obtained such that the dimensionless height $y^+ \leqslant 1$ is less than or equal to 1, with a growth rate of approximately 1.2. The distance Δs between the first mesh point and the hull surface can be expressed as follows:

$$\Delta s = \frac{y^+ L_{PP}}{Re\sqrt{\frac{C_f}{2}}} \tag{16}$$

where the friction coefficient, denoted as C_f, can be calculated using the formula provided by the International Towing Tank Conference [29]. Fig. 8 illustrates the distribution of y^+ on the hull obtained from CFD numerical simulations, with the average y^+ value being about 0.75.

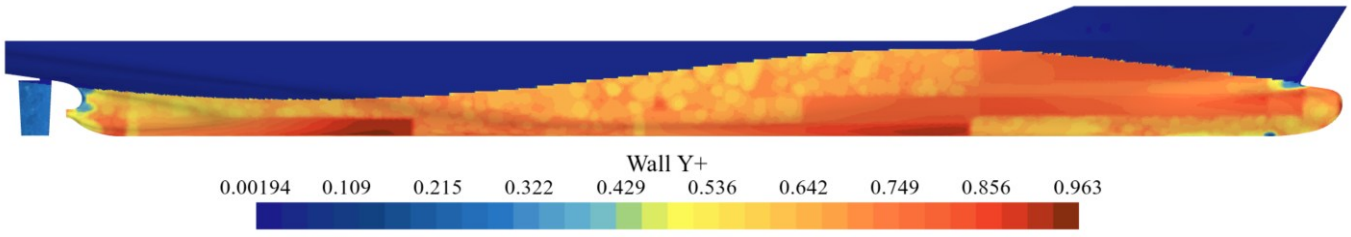

Fig. 8 y^+ distribution on the wall

3.3 Verification and Validation

To ensure sufficient accuracy in the numerical simulations of parametric rolling, this paper conducts validation and verification studies of the computational methods used. The research primarily focuses on investigating grid uncertainty and time step uncertainty to estimate the uncertainty in the computational results.

In the uncertainty analysis, this paper establishes three different mesh densities and three distinct time intervals. The base size ratios for the three meshes and time steps, defined as the uniform parameter refinement ratio r_i, are set to $\sqrt{2}$ and 2 respectively. Fig. 9 illustrates the three mesh scenarios used in the uncertainty study, where the surface mesh density, volume growth rate, and number of mesh layers vary between coarse, medium, and fine meshes.

Fig. 9 Three grid strategies for the KCS ship

Results obtained using fine, medium, and coarse meshes or time steps are denoted as S_1, S_2, and S_3, respectively. The convergence factor R can be defined as follows:

$$R = \frac{\varepsilon_{21}}{\varepsilon_{32}} = \frac{S_2 - S_1}{S_3 - S_2} \tag{17}$$

Based on the convergence factor R, three types of convergence criteria can be established:

(1) $0 < R < 1$; Monotonic convergence:

(2) $R < 0$; Oscillatory convergence:

(3) $R > 1$; divergence:

When monotonic convergence is achieved, Richardson's extrapolation method can be employed. The estimated numerical error δ_{RE}, precision order P_{RE}, and correction coefficient C_g can be calculated using the following formulas:

$$\delta_{RE} = \frac{\varepsilon_{21}}{r_i^{P_{RE}} - 1} \tag{18}$$

$$P_{RE} = \frac{\ln(\varepsilon_{32} / \varepsilon_{21})}{\ln r_i} \tag{19}$$

$$C_g = \frac{r_i P_{RE} - 1}{r_i P_{TH} - 1} \tag{20}$$

where P_{TH} represents the estimated order of computational precision as the interval approaches zero; typically $P_{TH} = 2$. The numerical error δ_{SN}, reference result S_C, and uncertainty $U_{G,T}$ can be estimated as follows:

$$\delta_{SN} = C_g \cdot \delta_{RE} \tag{21}$$

$$S_C = S - \delta_{SN} \tag{22}$$

$$U_{G,T} = \begin{cases} \left(9.6\left(1-C_g\right)^2 + 1.1\right)\left|\delta_{RE}\right|, & \left|1-C_g\right| < 0.125 \\ \left(2\left|1-C_g\right| + 1\right)\left|\delta_{RE}\right|, & \left|1-C_g\right| \geq 0.125 \end{cases} \tag{23}$$

Numerical uncertainty U_{SN}, comprises grid uncertainty U_G, time step uncertainty U_T, iterative uncertainty U_I, and uncertainty due to other parameters U_P. Based on prior research, iterative uncertainty U_I and uncertainty related to other parameters U_P are considered negligible compared to grid uncertainty U_G and time step uncertainty U_T.

$$U_{SN} = \sqrt{U_G^2 + U_T^2} \tag{24}$$

The validation uncertainty U_V can be represented as follows:

$$U_V = \sqrt{U_D^2 + U_{SN}^2} \tag{25}$$

where U_D represents the uncertainty of the experimental data, with $U_D = 2.00\%D$ in this paper.

Regarding the uncertainty analysis of parametric roll motion, the same conditions as the towing tank experiments are selected λ/L_{PP}=1.0, H_w/λ=0.02, and the KCS model ship is simulated at a cruising speed of V_m = 0.5 m/s. For the analysis of time step uncertainty, the medium time step is chosen as one 124th of the minimum encounter period. The results of the parametric roll numerical simulations across different mesh sizes and time step intervals are shown in Table 2. For the analyses of mesh spacing and time step interval uncertainty, the convergence factor R lies between 0 and 1, indicating monotonic convergence and suitability for Richardson extrapolation. The uncertainty analysis results presented in Table 3 indicate that the grid uncertainty for the parametric roll is 3.231%D and the time step uncertainty is 1.776% D, where D represents the experimental data. The results suggest that the simulation of ship parametric roll motion is particularly sensitive to mesh spacing.

Table 2 Results of parametric roll for the different grids and time steps

Grid	Cell (M)	Φ (deg)	Error %	Time step	$\triangle t$ (s)	Φ (deg)	Error %
Coarse	2.68	26.335	6.091	Coarse	0.012	26.455	6.575
Medium	5.08	25.701	3.537	Medium	0.006	25.701	3.537
Fine	10.07	25.402	2.333	Fine	0.003	25.612	3.179
EFD	—	24.823	—	EFD	—	24.823	—

Table 3 Results of uncertainties analysis

	r_i	R	C_g	$U_{G,T}$(%D)	U_{SN}(%D)
Grid (G)	$\sqrt{2}$	0.476	1.104	3.231	3.687
Time step (T)	2	0.120	2.456	1.776	

Table 4 presents the results of the validation study. According to the outcomes of the validation study, it is observed that all values of E are less than those of U_V, indicating that the computational results have been validated in terms of U_V.

Table 4 Results of the validation study

	U_{SN} (%D)	U_D (%D)	U_V (%D)	E (%D)
Φ	3.687	2	4.194	3.537

4. Results and discussion

4.1 Compare simulation results with experiments

This paper employs the Computational Fluid Dynamics approach to forecast the parametric roll motion of a KCS vessel facing head seas, with simulation conditions detailed in Table 5. Fig. 10 and Fig. 11 display the comparison between the numerical simulation results and experimental data for parametric roll under conditions of H_w/λ=0.02, λ/L_{PP}=1.0, and λ/L_{PP}=1.15. It is observed that the maximum error in the steady-state roll angle, compared to experimental values, is 4.7%. Therefore, using CFD to predict the parametric roll motion of container ships in the head seas achieves high accuracy.

Table 5 Simulation conditions

Wave steepness H_w/λ	Wave direction	Wave length λ/L_{PP}	Speed Vm(m/s)	Re
0.02	180°	1.0	0.3	6.83E+05
			0.4	9.11E+05
			0.5	1.14E+06
			0.6	1.37E+06
		1.15	0.4	9.11E+05
			0.5	1.14E+06
			0.6	1.37E+06
			0.7	1.59E+06
			0.8	1.82E+06

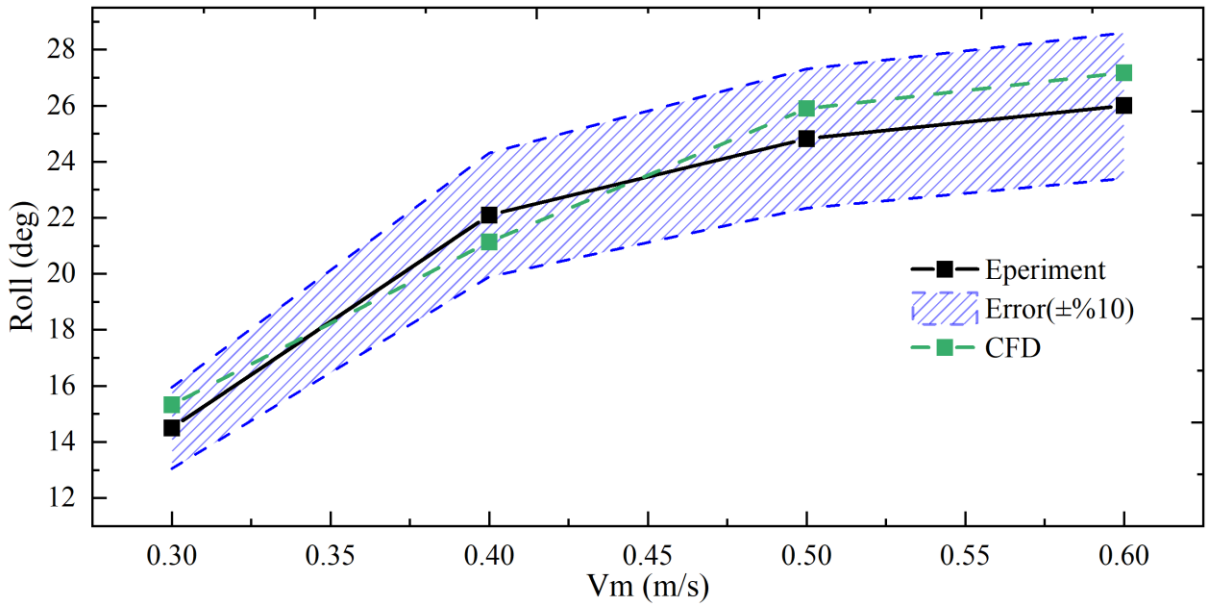

Fig. 10 Comparison of numerical results and experimental data when λ/L_{PP}=1.0

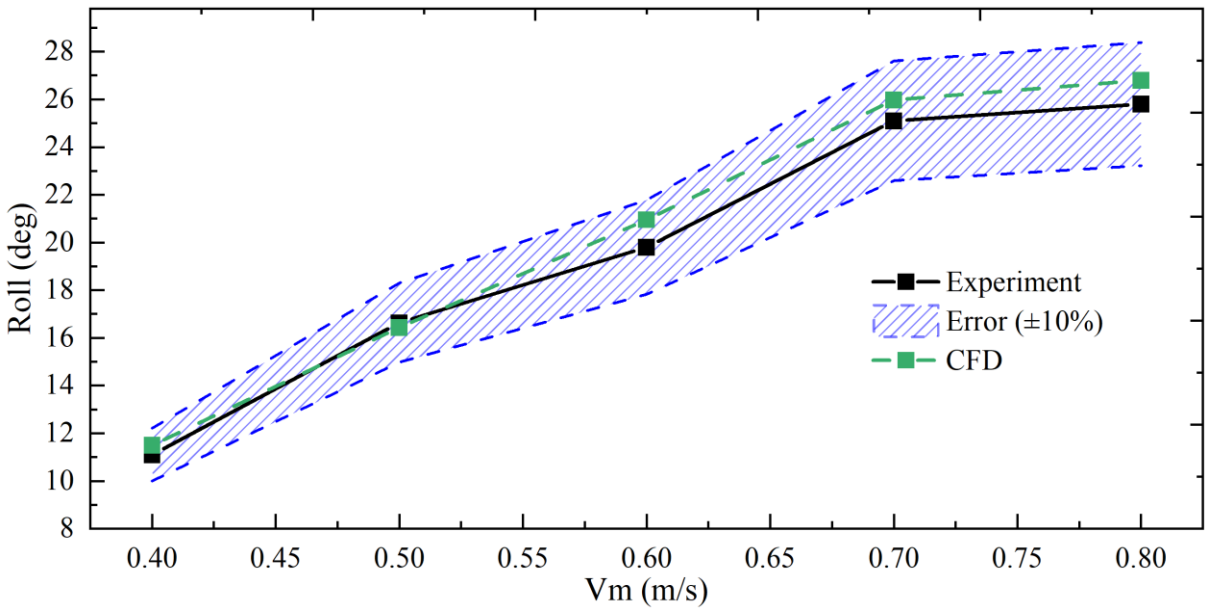

Fig. 11 Comparison of numerical results and experimental data when λ/L_{PP}=1.15

Fig. 12 and Fig.13 show the time history curves of parametric roll motion for the KCS vessel in head seas with regular waves. Observations indicate that the roll angle reaches a peak in a short period, and the numerical simulation results align well with the experimental data. However, there are variations in the roll period between the numerical simulations and experimental roll time history curves. This discrepancy may be attributed to changes in the roll period of the test ship caused by alterations in heading during the model tests using an autopilot.

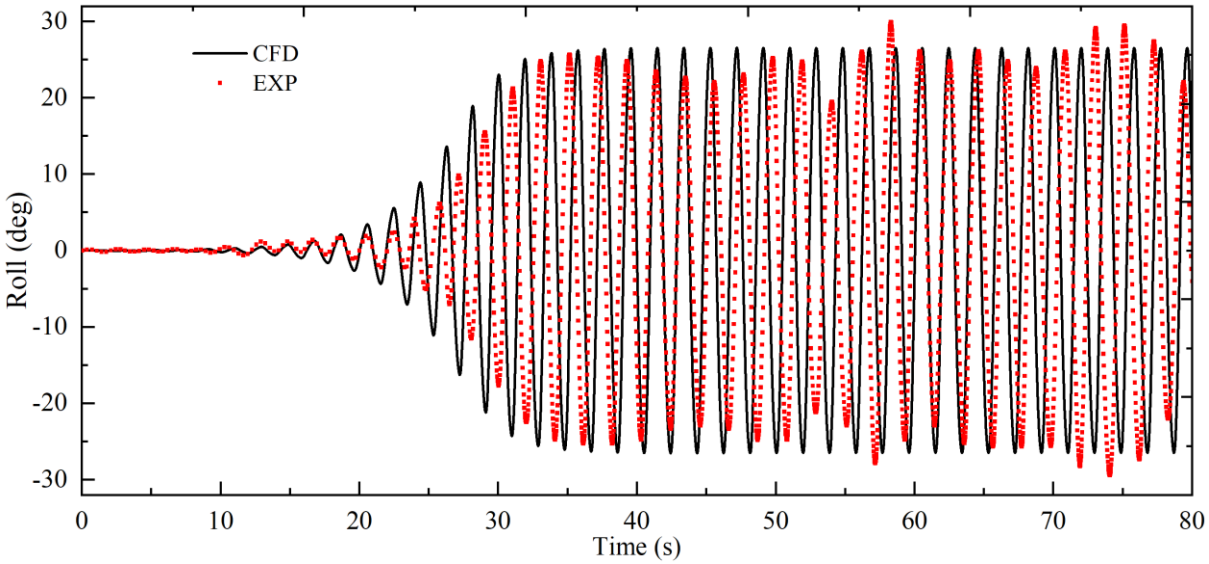

Fig. 12 Comparison of roll motion time histories from CFD simulations and experimental data at λ/L_{PP}=1.0, V_m=0.5m/s

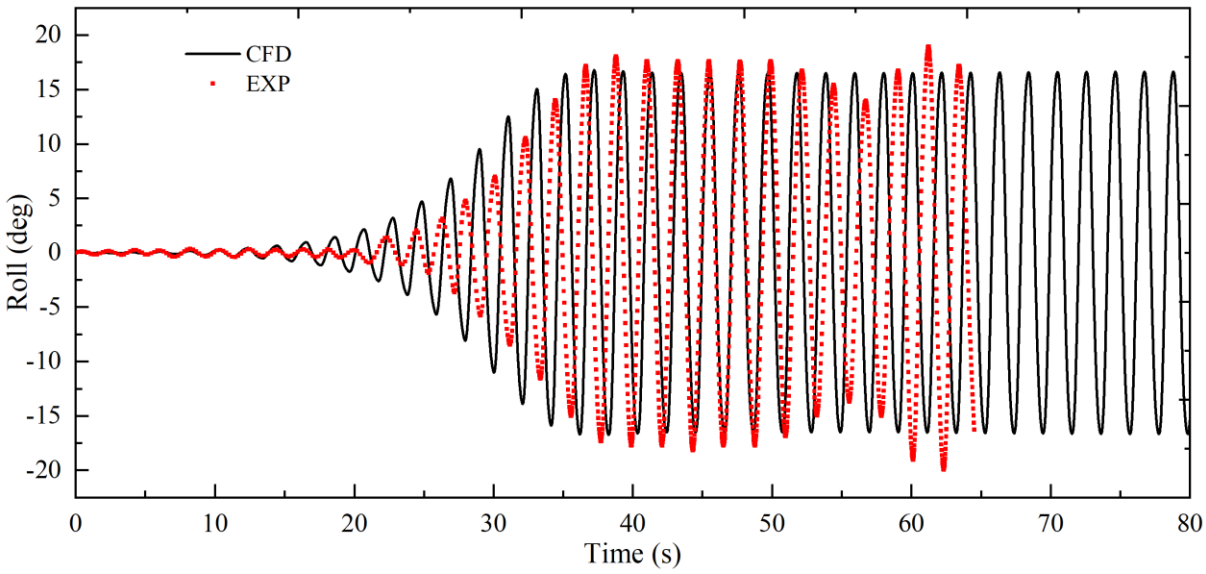

Fig. 13 Comparison of roll motion time histories from CFD simulations and experimental data at λ/L_{PP}=1.15, V_m=0.5m/s

4.2 The effect of initial roll angle on parametric roll

When ships navigate through waves, they may be subjected to disturbances from external environmental loads, causing them to encounter waves at a specific roll angle. To explore the impact of starting angles on the parametric roll movement of container vessels in head waves, this study established three initial roll angles of 5°, 10°, and 20°, serving as the initial disturbances for the parametric roll motion.

Under conditions of H_w/λ=0.02, λ/L_{PP}=1.0, and V_m=0.6m/s, the numerical simulation results for different initial disturbances are illustrated in Fig. 14. It can be found that three different initial roll angles trigger parametric roll responses with different frequencies. This is because the initial roll angle determines the initial kinetic and potential energies of the roll motion. When the initial roll angle is large, the vessel possesses higher initial kinetic and potential energies. Due to the increased initial kinetic energy, the rate of energy transformation during the parametric roll motion is accelerated, potentially leading to a higher frequency. Moreover, the substantial initial potential energy influences the vessel's restorative and damping characteristics during roll motion, thereby affecting the parametric roll response frequency.

In the same working situation, the numerical simulation results without initial roll angle are shown in Fig. 15. Upon comparison, it is observed that the maximum steady-state roll reached 27.1 ° for the influence of three different initial angles, which is almost the same as the maximum rolling angle in the case of no initial roll angle. With an initial roll angle of 5°, which is slowly increasing over time and takes the longest time to reach a steady state. Conversely, with an initial roll angle of 20°, the roll angle increases most rapidly, achieving stability in the shortest time. The study findings indicate that the initial roll angle does not affect the amplitude of the parametric roll at a steady state, but it does influence the time required to reach a stable condition. The larger the initial roll angle, the shorter the time to reach the steady state stage. It is worth noting that using the initial roll angle only validates the experimental results and does not predict the parametric rolling. This is due to the fact that the initial perturbation changes the course of the parameter rolling. Sadat-Hosseini [30] also fixed the model of the ONRT ship at a 30° initial roll angle during parametric roll model tests. In the study, the starting angle is set to 20° to achieve a quicker onset of parametric roll phenomena.

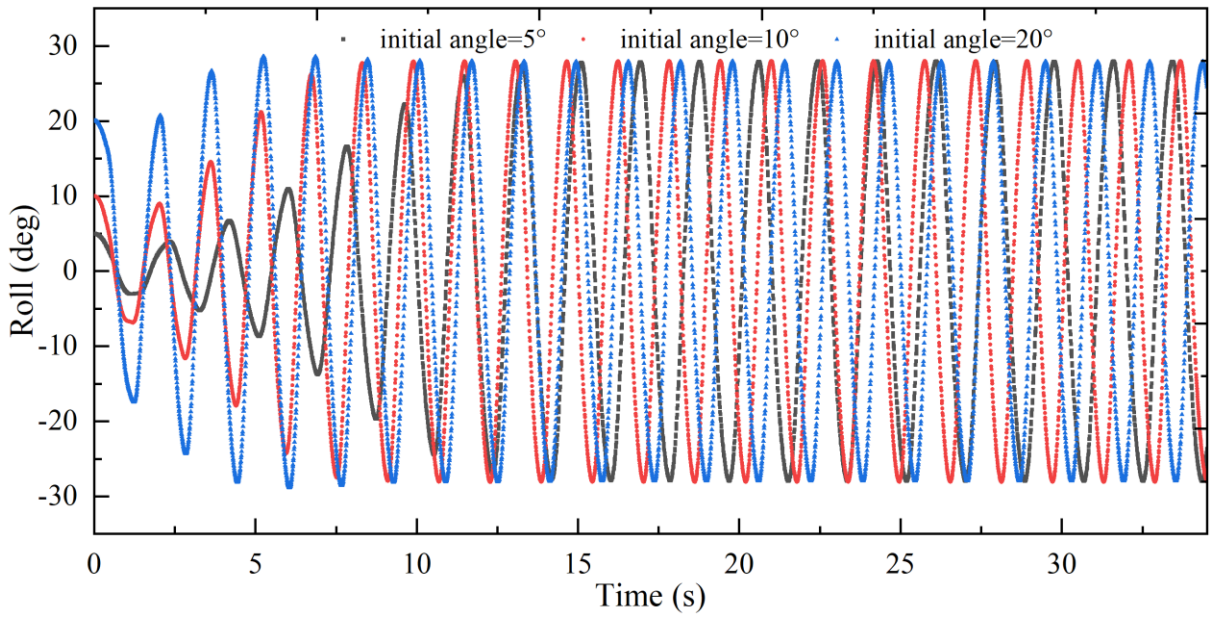

Fig. 14 Time history curves of parametric rolling under different initial roll angles

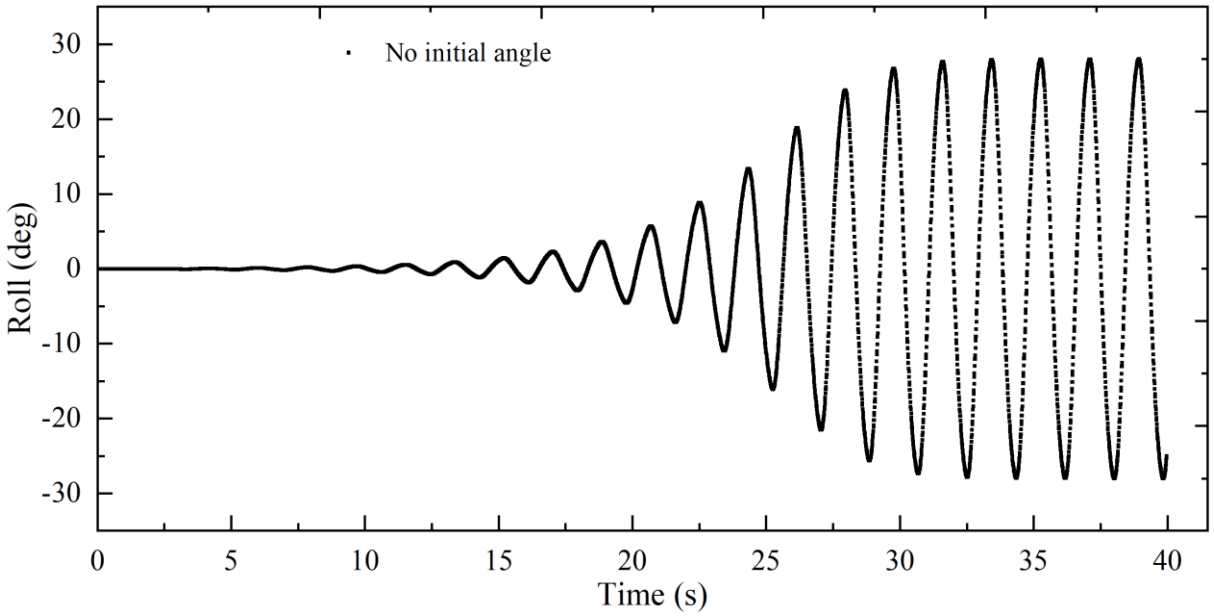

Fig. 15 Parametric roll motion time history curve without an initial roll angle

4.3 The effect of encounter frequency

During navigation, ships encounter waves at varying frequencies. The encounter frequency can be expressed as:

$$f_e = f_w + \frac{2\pi f_w^2}{g} V_m \tag{27}$$

where f_w represents the wave frequency.

This study investigates the impact of the ratio between encounter frequency and the ship's natural roll frequency on parametric rolling under head sea conditions, with wave steepness values of 0.02 and 0.025, and ship speeds ranging from 0.1 m/s to 0.6 m/s. Fig. 16 illustrates the occurrence of parametric rolling under different wave length-to-ship length ratios and varying ship speeds. It can be observed that parametric rolling is more likely to happen when the proportion of the encounter frequency to the natural rolling frequency of

the ship is close to 2. For conditions with excessively high or low speeds, where this ratio is significantly greater or less than 2, the occurrence of parametric rolling is unlikely. Furthermore, Fig. 16 also shows that the probability of the parameter rolling increases as the wavelength approaches the hull length.

The parametric roll motion under conditions of λ/L_{PP}=1.0 and V_m=0.5m/s was simulated using CFD methods, with the wave patterns around the model shown in Fig. 17. The figure presents snapshots at four typical moments, clearly illustrating the parametric rolling phenomenon. Due to the significant roll angle, deck wetting occurred at the midship section.

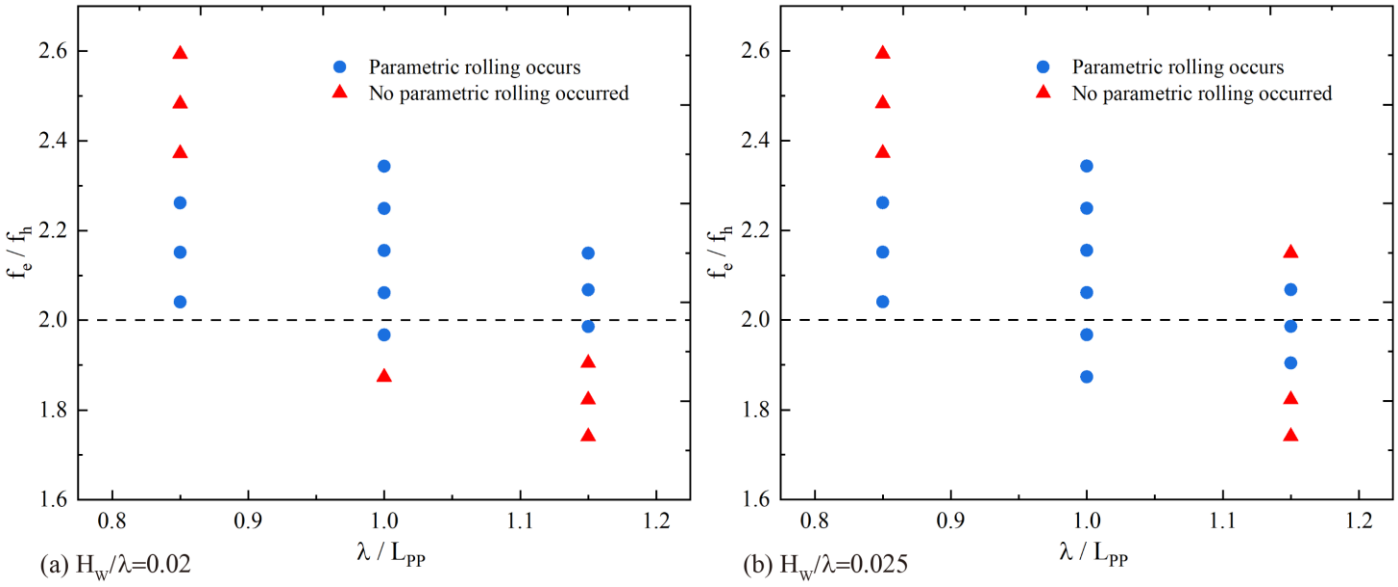

Fig. 16 The relationship between the occurrence of parametric rolling and f_e/f_h

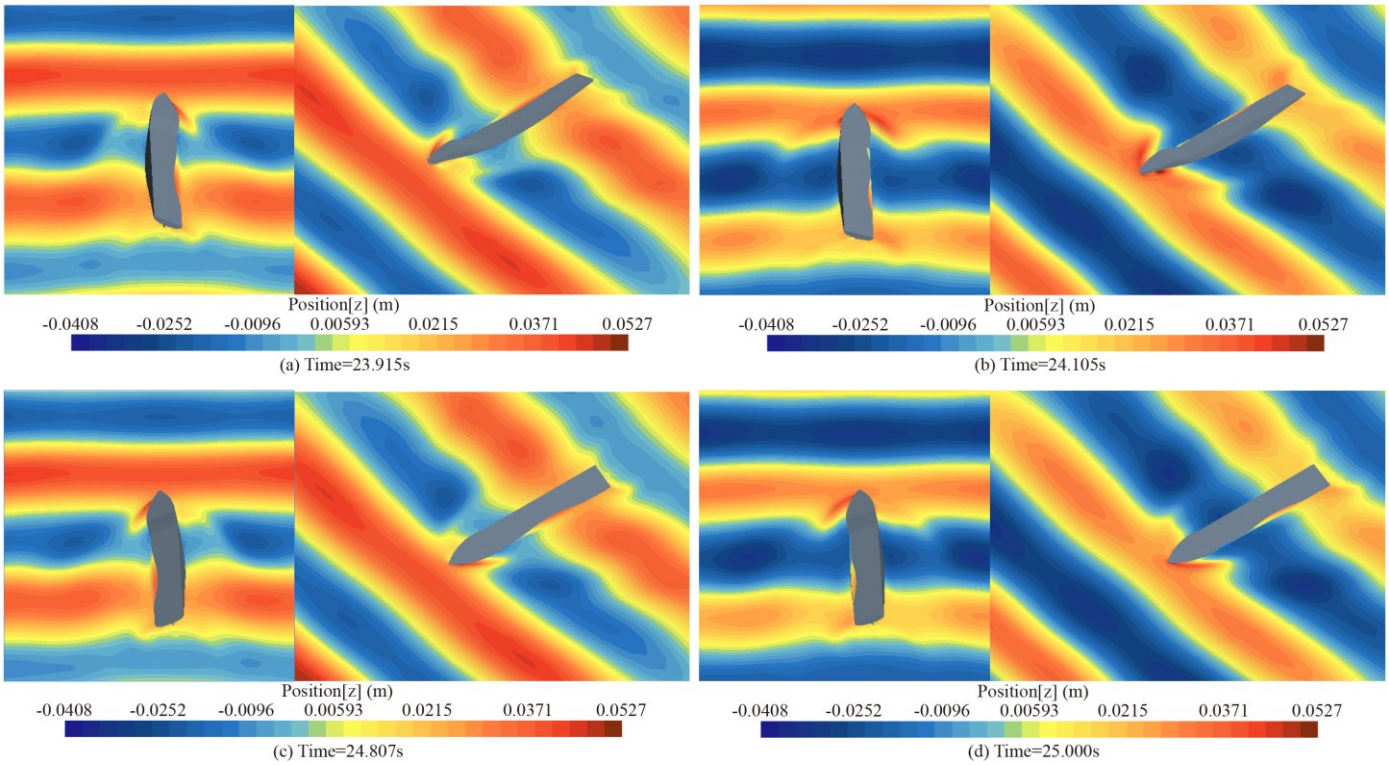

Fig. 17 Wave patterns generated during the parametric rolling motion of the KCS vessel in head seas

4.4 The effect of bilge keels

Bilge keels, as the most widely used roll-damping devices, offer the advantages of simple structure, low cost, and easy installation. Therefore, this study selects bilge keels as the roll-damping devices for the KCS vessel. Fig. 18 and Fig. 19 present the numerical simulation results of the roll, pitch, and heave motions for the KCS ship with and without bilge keels. The conditions selected are λ/L_{PP}=1.0, H_W/λ=0.02, V_m=0.4 m/s and λ/L_{PP}=1.15, H_W/λ=0.02, V_m=0.5m/s. According to the results, the installation of bilge keels significantly improves the parametric roll motion of the KCS vessel. For example, under the first condition, the maximum steady-state roll angle without bilge keels was 20.21°. However, with bilge keels installed, the maximum steady-state roll angle was reduced to 7.67°, and the occurrence of parametric rolling was also delayed. For pitch and heave motions, no significant changes were observed after the installation of bilge keels.

To further investigate the roll damping mechanism provided by bilge keels, Fig. 20 displays velocity vectors at the midship section both with and without bilge keels installed. The comparison reveals significant vortex formation at the site of the bilge keels following their installation. The generation and shedding of these vortices consume energy, which is effectively extracted from the roll motion of the ship. Therefore, the creation of vortices enhances the system damping, subsequently reducing both the amplitude and velocity of the roll. This damping effect is achieved by increasing hydrodynamic losses associated with the ship's motion, thereby reducing the energy involved in the roll.

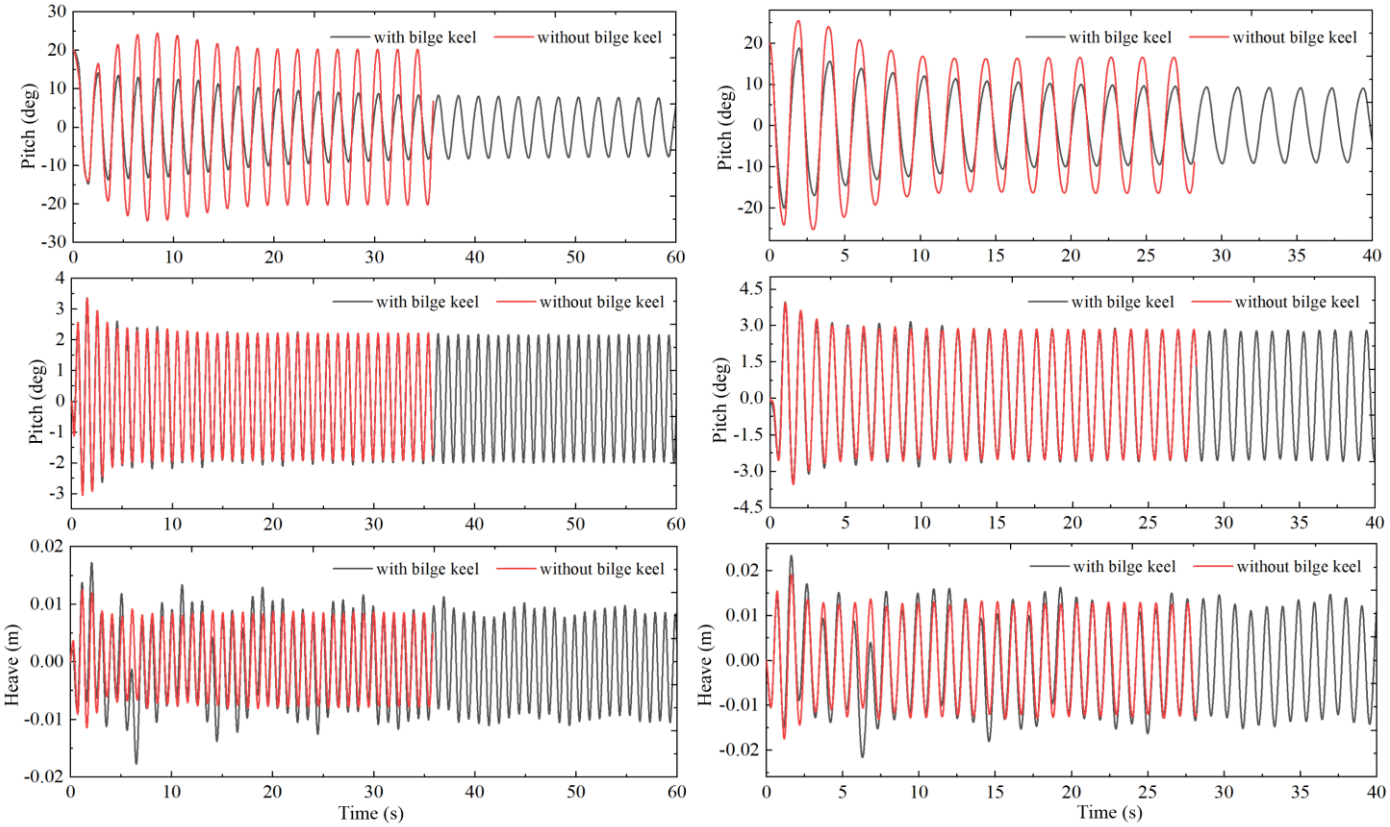

(a) λ/L_{PP}=1.0、H_W/λ= 0.02、V_m= 0.4m/s (b) λ/L_{PP}= 1.15、H_W/λ= 0.02、V_m= 0.5m/s

Fig. 18 Time history of roll, pitch, and heave motions for the KCS ship with bilge keels in head seas

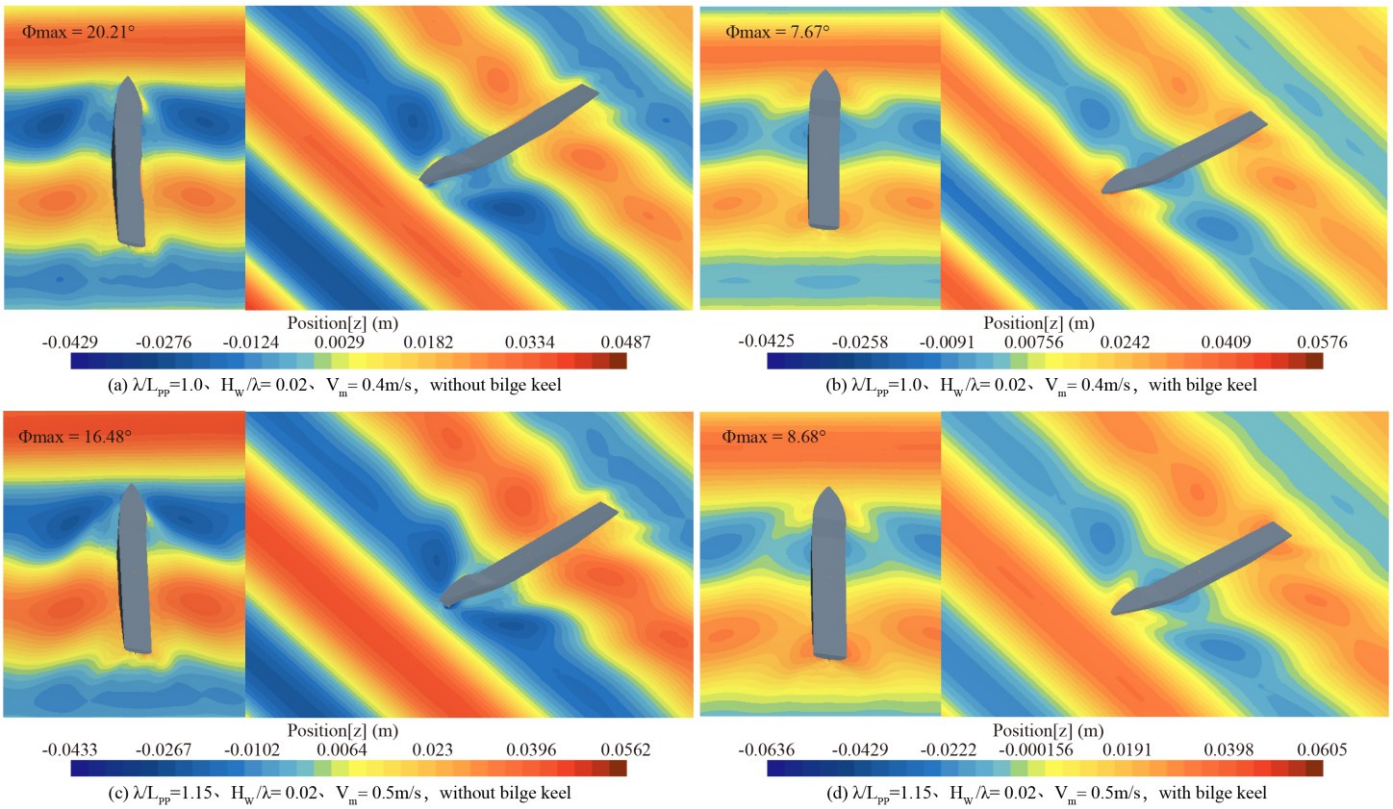

Fig. 19 Wave patterns generated during parametric rolling of the KCS ship with bilge keels in head seas

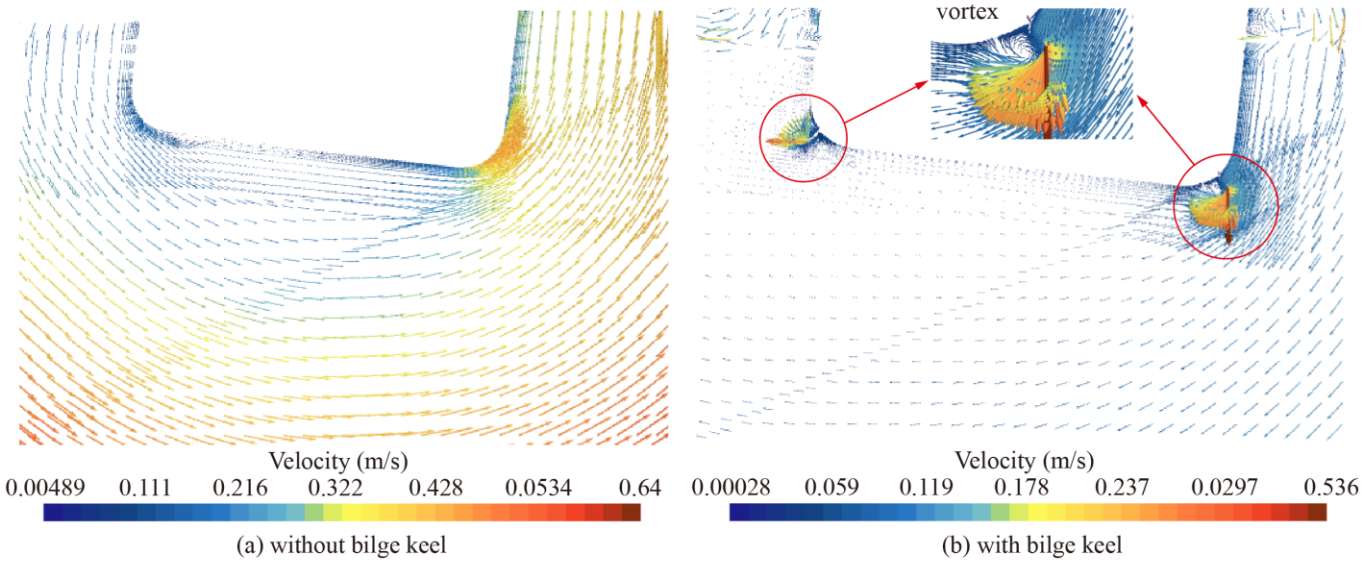

Fig. 20 Velocity vector diagram at the midship section of the KCS ship

5. Conclusion

This paper employs the unsteady RANS approach combined with dynamic overset grid technology to conduct numerical simulations of parametric roll motion for a container ship in head sea conditions and investigates the roll-reducing mechanism of bilge keels. Based on the research conducted, the paper arrives at the following conclusions:

1. A comparison between the CFD simulation results of parametric roll motion for the KCS ship in head seas and experimental data reveals a maximum discrepancy of 4.7% in the steady-state roll angle, which meets

the requirements of the IMO. This demonstrates the reliability of using CFD methods to predict parametric roll motion in container ships.

2. This study selected three different initial roll angles to investigate the impact of initial disturbances on parametric rolling. The research indicates that the initial angle does not impact the amplitude of the parametric roll at the steady state; however, it influences the time required to reach a stable condition. The greater the angle of the initial roll, the shorter the time needed to achieve stability.

3. A study on the occurrence of parametric rolling under conditions of varying wave-to-ship length ratios and different speeds reveals that this phenomenon is likely when the ratio of encounter frequency to the natural roll frequency of the ship approaches 2. Under conditions where speeds are excessively high or low, and the proportion of encounter frequency to the ship's natural roll frequency is significantly greater or less than 2, parametric rolling tends to be unlikely. Moreover, the likelihood of a parameter roll increases as the wavelength approaches the captain.

4. After the installation of bilge keels, there is a significant reduction in the maximum roll amplitude at steady state, and the occurrence of parametric rolling is also delayed. For pitch and heave motions, there are no noticeable changes after the installation of bilge keels. Prominent vortices form at the location of the bilge keels following their installation. The generation and shedding of these vortices consume energy, thereby reducing the amplitude and velocity of the roll.

ACKNOWLEDGEMENT

The authors gratefully acknowledge the support from the Shanghai Municipal Science and Technology Commission Local College Capacity Building Project (Z20228005), National Natural Science Foundation of China (Grant Nos. 51779135 and 51009087) and Shanghai Natural Science Foundation of China (project approval number: 14ZR1419500).

REFERENCES

[1] Maruyama, Y., Maki, A., Dostal, L., Umeda, N., 2022. Improved stochastic averaging method using Hamiltonian for parametric rolling in irregular longitudinal waves. *Journal of Marine Science and Technology*, 27(1), 186-202. https://doi.org/10.1007/s00773-021-00824-y

[2] Ribeiro e Silva, S., Turk, A., Soares, C. G., 2010. On the parametric rolling of container vessels. *Brodogradnja*, 61(4), 347-358.

[3] Chen, X., Zhu, R.-C., Zhou, W.-J., Zhao, J., 2018. A 3D multi-domain high order boundary element method to evaluate time domain motions and added resistance of ship in waves. *Ocean Engineering*, 159, 112-128. https://doi.org/10.1016/j.oceaneng.2018.03.091

[4] Li, Y., Su, M., Li, H., Deng, R., Wang, K., Hu, Z., 2019. Numerical research on time domain ship motions coupled with sloshing at different liquid levels and forward speeds. *Ocean Engineering*, 178, 246-259. https://doi.org/10.1016/j.oceaneng.2019.02.063

[5] Ribeiro e Silva, S. R., Soares, C. G., 2013. Prediction of parametric rolling in waves with a time domain non-linear strip theory model. *Ocean Engineering*, 72, 453-469. https://doi.org/10.1016/j.oceaneng.2013.07.011

[6] Hu, K., Wang, R., Ma, S., Duan, W., Xu, W., Deng, R., 2017. Numerical modelling and study of parametric rolling for C11 containership in regular head seas using consistent strip theory. *Brodogradnja*, 68(3), 135-156. https://doi.org/10.21278/brod68309

[7] Coslovich, F., Kjellberg, M., Janson, C.-E., 2019. Prediction of parametric rolling for a container ship in regular and irregular waves using a fully nonlinear time domain potential flow method. *Proceedings of the 8th International Conference on Computational Methods in Marine Engineering, MARINE 2019*, 13-15 May, Göteborg, Sweden.

[8] Ghamari, I., Greco, M., Faltinsen, O. M., Lugni, C., 2020. Numerical and experimental study on the parametric roll resonance for a fishing vessel with and without forward speed. *Applied Ocean Research*, 101, 102272. https://doi.org/10.1016/j.apor.2020.102272

[9] Zhou, Y.-H., Ning, M., Jiang, L., Min, G., 2016. A study of hybrid prediction method for ship parametric rolling. *Journal of Hydrodynamics*, 28(4), 617-628. https://doi.org/10.1016/S1001-6058(16)60666-2

[10] Yıldız, B., Şener, B., Yurtseven, A., Katayama, T., 2019. Numerical and experimental calculation of roll amplitude effect on roll damping. *Brodogradnja*, 70(2), 1-15. https://doi.org/10.21278/brod70201

[11] Hashimoto, H., Omura, T., Matsuda, A., Yoneda, S., Stern, F., Tahara, Y., 2019. Several remarks on EFD and CFD for ship roll decay. *Ocean Engineering*, 186, 106082. https://doi.org/10.1016/j.oceaneng.2019.05.064

[12] Kianejad, S. S., Enshaei, H., Duffy, J., Ansarifard, N., Ranmuthugala, D., 2019. Ship roll damping coefficient prediction using CFD. *Journal of Ship Research*, 63(02), 108-122. https://doi.org/10.5957/JOSR.07220021

[13] Wang, S., Wei, J., Chen, X., Liu, L., Zhang, Z., 2019. Numerical simulations of KCS parametric rolling in head waves. International Conference on Offshore Mechanics and Arctic Engineering, Wuhan, China. https://doi.org/10.1115/OMAE2019-95563

[14] Zhang, W., Liu, Y.-D., Chen, C., He, Y.-P., Tang, Y.-Y., Sun, J.-J. 2023. Research on the parametric rolling of the KCS container ship. *Journal of Marine Science and Technology*, 28(3): 675-688. https://doi.org/10.1007/s00773-023-00948-3

[15] Li, H., Sun, Z., Han, B., Shao, Y., Deng, B., 2022. Research on the motion response of aquaculture ship and tank sloshing under rolling resonance. *Brodogradnja*, 73(2), 1-15. https://doi.org/10.21278/brod73201

[16] Liu, L., Chen, M., Wang, X., Zhang, Z., Yu, J., Feng, D., 2021. CFD prediction of full-scale ship parametric roll in head wave. *Ocean Engineering*, 233, 109180. https://doi.org/10.1016/j.oceaneng.2021.109180

[17] Liu, L., Feng, D., Wang, X., Zhang, Z., Yu, J., Chen, M., 2022. Numerical study on the effect of sloshing on ship parametric roll. *Ocean Engineering*, 247, 110612. https://doi.org/10.1016/j.oceaneng.2022.110612

[18] Schumacher, A., E Silva, S. R., Soares, C. G., 2016. Experimental and numerical study of a containership under parametric rolling conditions in waves. *Ocean Engineering*, 124, 385-403. https://doi.org/10.1016/j.oceaneng.2016.07.034

[19] Lu, J., Gu, M., Umeda, N., 2017. Experimental and numerical study on several crucial elements for predicting parametric roll in regular head seas. *Journal of Marine Science and Technology*, 22, 25-37. https://doi.org/10.1007/s00773-016-0391-0

[20] Ma, S., Ge, W.-P., Ertekin, R., He, Q., Duan, W.-Y., 2018. Experimental and numerical investigations of ship parametric rolling in regular head waves. *China Ocean Engineering*, 32(4), 431-442. https://doi.org/10.1007/s13344-018-0045-6

[21] Yu, L., Taguchi, K., Kenta, A., Ma, N., Hirakawa, Y., 2018. Model experiments on the early detection and rudder stabilization of KCS parametric roll in head waves. *Journal of Marine Science and Technology*, 23, 141-163. https://doi.org/10.1007/s00773-017-0463-9

[22] Kapsenberg, G., Wandji, C., Duz, B., Kim, S., 2020. A comparison of numerical simulations and model experiments on parametric roll in Irregular Seas. *Journal of Marine Science and Engineering*, 8(7), 474. https://doi.org/10.3390/jmse8070474

[23] Zhou, Y.-H., Sun, Q., Shi, X., 2022. Experimental and numerical study on the parametric roll of an offshore research vessel with extended low weather deck. *Ocean Engineering*, 262, 111914. https://doi.org/10.1016/j.oceaneng.2022.111914

[24] Pesman, E., Copuroglu, H. I., Katayama, T., 2024. The effect of a ship's acceleration and deceleration on parametric roll motion in regular head waves at resonance conditions. *Ocean Engineering*, 291, 116367. https://doi.org/10.1016/j.oceaneng.2023.116367

[25] Saydam, A. Z., Küçüksu, G. N., İnsel, M., Gökçay, S., 2022. Uncertainty quantification of self-propulsion analyses with RANS-CFD and comparison with full-scale ship trials. *Brodogradnja*, 73(4), 107-129. https://doi.org/10.21278/brod73406

[26] Pena, B., Muk-Pavic, E., Thomas, G., Fitzsimmons, P., 2020. An approach for the accurate investigation of full-scale ship boundary layers and wakes. *Ocean Engineering*, 214, 107854. https://doi.org/10.1016/j.oceaneng.2020.107854

[27] Hadi, E. S., Tuswan, T., Azizah, G., Ali, B., Samuel, S., Hakim, M. L., Hadi, M. R. C. P., Iqbal, M., Sari, D. P., Satrio, D. 2023. Influence of the canal width and depth on the resistance of 750 DWT Perintis ship using CFD simulation. *Brodogradnja*, 74(1), 117-144. https://doi.org/10.21278/brod74107

[28] Yu, L., Ma, N., Wang, S., 2019. Parametric roll prediction of the KCS containership in head waves with emphasis on the roll damping and nonlinear restoring moment. *Ocean Engineering*, 188, 106298. https://doi.org/10.1016/j.oceaneng.2019.106298

[29] ITTC, 2014. Practical Guidelines for Ship CFD Applications. https://www.ittc.info/media/9773/75-03-02-03.pdf

[30] Sadat-Hosseini, H., Stern, F., Olivieri, A., Campana, E. F., Hashimoto, H., Umeda, N., Bulian, G., Francescutto, A., 2010. Head-wave parametric rolling of a surface combatant. *Ocean Engineering*, 37(10), 859-878. https://doi.org/10.1016/j.oceaneng.2010.02.010